Evidence Based Detection of Spiculated Masses and Architectural Distortions

Mehul P. Sampat[a], Gary J. Whitman[b]
Mia K. Markey[a♦] and Alan C. Bovik[c]
[a]Department. of Biomedical Engineering, The University of Texas at Austin, Austin, TX 78712, USA
[b]Division of Diagnostic Imaging, The University of Texas M. D. Anderson Cancer Center, Houston, TX 77030, USA
[c]Department. of Electrical and Computer Engineering, The University of Texas at Austin, Austin, TX 78712, USA

ABSTRACT

Mass detection algorithms generally consist of two stages. The aim of the first stage is to detect all potential masses. In the second stage, the aim is to reduce the false-positives by classifying the detected objects as masses or normal tissue. In this paper, we present a new evidence based, stage-one algorithm for the detection of spiculated masses and architectural distortions. By evidence based, we mean that we use the statistics of the physical characteristics of these abnormalities to determine the parameters of the detection algorithm. Our stage-one algorithm consists of two steps, an enhancement step followed by a filtering step. In the first step, we propose a new technique for the enhancement of spiculations in which a linear filter is applied to the Radon transform of the image. In the second step, we filter the enhanced images with a new class of linear image filters called Radial Spiculation Filters. We have invented these filters specifically for detecting spiculated masses and architectural distortions that are marked by converging lines or spiculations. These filters are highly specific narrowband filters, which are designed to match the expected structures of these abnormalities and form a new class of wavelet-type filterbanks derived from optimal theories of filtering. A key aspect of this work is that each parameter of the filter has been incorporated to capture the variation in physical characteristics of spiculated masses and architectural distortions and that the parameters of the stage-one detection algorithm are determined by the physical measurements.

Keywords: Radon Transform, Radial Spiculation Filters, breast cancer, mammography, computer-aided detection and diagnosis.

1. INTRODUCTION

The American Cancer Society estimates that 215,990 women will be diagnosed with breast cancer in the U.S. in 2004 [1] and 40,110 women will die of the disease. In the US, breast cancer is the most common form of cancer among women and is the second leading cause of cancer deaths, after lung cancer [1]. Women in the U.S. have about a 1 in 8 lifetime risk of developing invasive breast cancer [2, 3]. Early detection of breast cancer increases the treatment options for patients and also increases the survival rate.

Screening mammography, x-ray imaging of the breast, is currently the most effective tool for early detection of breast cancer. Screening mammographic examinations are performed on asymptomatic woman to detect early, clinically unsuspected breast cancer. Two views of each breast are recorded; the craniocaudal (CC) view, which is a top to bottom view, and a mediolateral oblique (MLO) view, which is a side view taken at an angle.

Radiologists visually search mammograms for specific abnormalities. Some of the important signs of breast cancer that radiologists look for are clusters of microcalcifications, masses, and architectural distortions. Calcifications are tiny deposits of calcium, which appear as small bright spots on the mammogram. They are characterized by their type and distribution properties. A mass is defined as a space-occupying lesion seen in at least two different projections [4]. Masses are described by their shape and margin characteristics. An architectural distortion is defined as follows:

♦ mia.markey@mail.utexas.edu; phone: +1.512.471.1771; fax: +1.512.471.0616; http://www.bme.utexas.edu/research/informatics/

"The normal architecture is distorted with no definite mass visible. This includes spiculations radiating from a point, and focal retraction or distortion of the edge of the parenchyma" [4].

Breast lesions are described and reported according to the Breast Imaging Reporting and Data System (BI-RADS™) [4]. BI-RADS™ is a mammography lexicon developed by the American College of Radiology (ACR), for the description of mammographic lesions. The BI-RADS™ lexicon includes descriptors such as the margin of a mass and the distribution of calcifications and it defines final assessment categories to describe the radiologist's level of suspicion about the mammographic abnormality. It has been demonstrated that the BI-RADS™ final assessment rating is an indicator of the likelihood of malignancy [5]. If a suspicious abnormality is detected, a diagnostic mammographic examination is carried out to decide the future course of action required. Based on the level of suspicion of the abnormality following the diagnostic examination, a recommendation is made for routine follow up, short-term follow up, or biopsy.

Early detection via mammography increases breast cancer treatment options and the survival rate [6]. However, mammography is not perfect. Detection of suspicious abnormalities is a repetitive and fatiguing task. For every thousand cases analyzed by a radiologist, only 3 to 4 are cancerous and thus an abnormality may be overlooked. As a result, radiologists fail to detect 10-30% of cancers [7-9]. Approximately two-thirds of these false-negative results are due to missed lesions that are evident retrospectively [10]. Due to the considerable amount of overlap in the appearance of malignant and benign abnormalities, mammography has a positive predictive value (PPV) of less than 35% [11], where the PPV is defined as the percentage of lesions subjected to biopsy that were found to be cancer. Thus, a high proportion of biopsies are performed on benign lesions. Avoiding benign biopsies would spare women anxiety, discomfort, and expense.

Computer-Aided Detection (CAD) systems have been developed to aid radiologists in detecting mammographic lesions that may indicate the presence of breast cancer [12-16]. These systems act only as a second reader and the final decision is made by the radiologist. Recent studies have also shown that CAD systems, when used as an aid, have improved radiologists' accuracy of detection of breast cancer. Computer-Aided Diagnosis (CADx) systems for aiding in the decision between follow-up and biopsy are still in development. It is important to realize that mammographic image analysis is an extremely challenging task for a number of reasons. First, since the efficacy of CAD/CADx systems can have very serious implications, there is a need for near perfection. Second, the large variability in the appearance of abnormalities makes this a very difficult image analysis task. Finally, abnormalities are often occluded or hidden in dense breast tissue, which makes detection difficult.

Masses with spiculated margins carry a much higher risk of malignancy than calcifications or other types of masses. Spiculated masses (SM) account for about 14% of biopsied lesions, and about 81% of these are malignant [17]. However, current CAD systems are dramatically better at detecting microcalcifications than masses. The most widely used commercial CAD system is reported to have 98.5% sensitivity at 0.185 false positives per image (FPI) for microcalcification clusters but only 86% sensitivity at 0.24 FPI for SM [18, 19]. The sensitivity is considerably lower for SM that are rated as "subtle" by radiologists (sensitivity of 52%) [19]. Moreover, since current systems were devised with masses and calcifications in mind, they don't perform as well on other, less prevalent but still clinically significant lesion types, particularly architectural distortions (AD). It is estimated that 12-45% of cancers missed in mammographic screening are AD [9, 20, 21]. AD are strongly suggestive of malignancy; approximately 48-60% of the AD that are biopsied are found to be cancer [5, 22], and about 80% of those cancers are invasive [22]. A recent study of AD reported that one commercial CAD system achieved a per-image sensitivity of 30 / 80 = 38% at 0.70 FPI and another achieved 17 / 80 = 21% sensitivity at 1.27 FPI. Thus there is a need for improvement in the detection accuracy of spiculated masses and architectural distortions. In this work we have tried to develop an evidence based framework for the detection of these abnormalities based on their physical characteristics.

The organization of this paper is as follows. Section 2 describes the new stage-one algorithm, the data sets used and the physical measurements made. Section 3 discusses the measurement and detection results obtained. Finally, the concluding remarks and future work are presented in Section 4.

2. METHODS

Many mass detection algorithms consist of two stages. In the first stage, potential masses are detected whereas in the second stage, the number of false-positives are reduced by classifying the detected objects as masses or normal tissue. In this paper, we present a new stage-one algorithm for the detection of spiculated masses and architectural distortions based on their physical characteristics. This is one of the key contributions of this work. We made

preliminary measurements of a number of parameters such as the width and length of spicules, the number of spicules, lengths of the major and minor axes of the central mass region of spiculated masses.

The stage-one algorithm we have developed consists of an enhancement step followed by a detection step. The first step uses a new technique for the enhancement of spiculations in which a linear filter is applied to the Radon transform of the image. The filter parameters were set based on measurements made on a set of spiculated masses and architectural distortions. In the second step, the enhanced images are filtered with a new class of linear image filters, which we call, Radial Spiculation Filters. These filters have been invented specifically for detecting spiculated masses and architectural distortions, which are marked by converging lines or spiculations. The details of the two steps are given in sections 2.1and 2.2 respectively.

2.1. Enhancement of Spiculations

The most prominent feature of spiculated masses and architectural distortions is the presence of spicules radiating in all directions. The goal of this stage is to enhance spicules which can be approximated as linear structures. We model spicules as lines of a certain width or thickness. The Radon domain is a convenient space to detect lines. To enhance spicules, we propose a novel algorithm in which we compute the Radon transform of the image and then perform filtering in the Radon domain to enhance linear structures. The discrete Radon transform $\hat{g}(\rho,\theta)$, of an N x N image $f(x, y)$ is given by:

$$\hat{g}(\rho,\theta) = \sum_{y=-N/2}^{N/2} \sum_{x=-N/2}^{N/2} f(x,y)\delta(\rho - x\cos(\theta) - y\sin(\theta)) \quad \text{Equation 1}$$

Where $\delta(r)$ is the Kronecker impulse function, which is zero everywhere except when $r = 0$.
Hence, the term $\delta(\rho - x\cos(\theta) - y\sin(\theta))$ contributes summed values of $f(x,y)$ only along the line $\rho - x\cos(\theta) - y\sin(\theta)$ and thus the value of $\hat{g}(\rho,\theta)$ for any (ρ,θ) is the sum of values of $f(x,y)$ along this line.

Thus, a line in the image space $f(x, y)$ produces or maps to a peak in the Radon domain. We also note that lines of different thickness would have different representations in the Radon domain. Figure 2 show two lines of different thickness and their corresponding Radon transforms. The two lines have the same length of 255 pixels and each pixel on the line has a uniform intensity of 1. In the Radon domain, the row values correspond to the different values of ρ and the column values represent the different θ values. Thus, a single pixel thick line would be represented by a point in the Radon domain whereas a 4 pixel thick line would be represented by 4 points along a column in the Radon domain. Thus, by enhancing sharp changes or "local peaks" along the columns in the Radon domain, it is possible to detect the corresponding lines in the image. To do so, a number of peak detection algorithms can be used.

After filtering the Radon domain with the filter described above, each column of the filtered Radon domain is then thresholded to retain the largest peaks. Finally, the inverse Radon transform is computed by using the filtered back-projection algorithm [23], to obtain an image in which linear structures are enhanced. The inverse Radon transform can be computed using equations 2 and 3, where $S_\theta(\omega)$ is the one-dimensional Fourier transform of $g_\theta(\rho)$ [23].

$$f(x,y) = \frac{\pi}{K}\sum_{i=1}^{K} \hat{Q}_{\theta_i}(x\cos(\theta i) + y\sin(\theta i)) \quad \text{Equation (2)}$$

$$\hat{Q}_{\theta_i}\left(\frac{k}{2W}\right) \approx \frac{2W}{N}\sum_{m=-N/2}^{N/2} S_\theta\left(m\frac{2W}{N}\right)\left|m\frac{2W}{N}\right| e^{j2\pi(mk/N)} \quad \text{Equation (3)}$$

Thus, the output of the enhancement stage is an enhanced image and all subsequent processing will be performed on this image. The limitation of this algorithm is that it would enhance not only spiculations but all other linear structures in the image as well. A summary of the enhancement algorithm is shown in Figure 3.
Figure 4 clearly demonstrates the advantages of filtering the Radon domain.

2.2. Detection Using Radial Spiculation Filters

The goal of the enhancement stage described in section 2.1 is to enhance spiculations in mammograms. The aim of this stage is to detect the spatial locations where these spiculations converge. For this purpose, we have invented a new class of linear image filters that we term as Radial Spiculation filters (RSF), designed specifically for detecting spiculated masses and architectural distortions, which are characterized by converging spiculations. The basic idea is to design a "matched filter" for a spiculated mass or architectural distortion. That is, once the enhanced image is processed with these filters, a large output would be obtained when the filters are "tuned to" or "match" a spiculated mass or architectural distortion. We define two classes of RSF called, the Cosine Radial Spiculation Filters (CRSF) and Sine Radial Spiculation Filters (SRSF). These are defined as follows:

$$\text{CSRF:} \quad f_c(x,y) = g(r_0,\sigma)\cos(\omega\theta) \quad \text{Equation (4)}$$

$$\text{SRSF:} \quad f_s(x,y) = g(r_0,\sigma)\sin(\omega\theta) \quad \text{Equation (5)}$$

$$g(r_0,\sigma) = \exp\left[-(r - r_0)^2 / (2\sigma^2)\right] \quad \text{Equation (6)}$$

Where $r^2 = x^2 + y^2$ and $\theta = \arctan(y/x)$, r_0 is the radius in pixels, σ is the standard deviation in pixels and ω is the frequency in cycles per circumference.

A cosine and sine radial spiculation filter pair is shown in Figure 5. The goal of using these filters is to localize a SM or AD by detecting the spatial locations where the spicules converge. These filters are highly specific narrowband filters which have been designed to match stellate patterns of spiculations. This new class of wavelet-type filterbanks is derived from optimal theories of filtering and is designed to match the expected structures of spiculated lesions. There are large variations in the shape and size of SM's and AD's. To account for this variability, three parameters, (r_0, σ, ω) have been used to define each filter. Each parameter has been incorporated in the filter to capture a particular physical characteristic of SM's and AD's and the motivation for including these is as follows:

r_0: It is known that spiculated masses have different sizes and their diameters can vary from 4 mm to 4 cm [24]. A filter can be "matched" to masses of different sizes by varying the parameter r_0. This parameter controls the radius of the filter.

ω: The number of spiculations on a spiculated mass and architectural distortion varies tremendously. To capture a SM/AD with few spiculations, a filter with a low frequency should be used as it would be a better match than a high frequency filter. Similarly, a high frequency filter should be used to capture a SM/AD with many spicules. The maximum value of ω depends on the minimum value of r_0. If the minimum value of r_0 is $r_{\min}$, then the maximum value of ω is equal to $\pi \cdot r_{\min}$.

A set of filters are shown in Figure 6. Since our goal is to design "matched filters", we see that such a set matches a SM or AD much more than a single filter. This is because the spicules of SM or AD can be thought of as radiating "outwards" from a central point and thus such a set or bank of filters is better suited for the detection task. We define such a set of filters as a Radial Spiculation Filter Bank (RSFB). A Cosine Spiculation Filter Bank (CRSFB) as a set of CRSF's with same values of σ and frequency ω and with increasing values of r_0. The value of r_0 is increased so that the filters of a bank intersect at half-peak.

We now describe how a CRSFB and its corresponding SRSFB can be used for the detection of masses. Let $OPsin$ and $OPcos$ be the output obtained after filtering the enhanced image with a pair of the sine and cosine filters respectively. The sine and cosine filters form a pair of quadrature filters. The responses of the cosine and sine filters are identical except for a phase difference of π/2. The advantage of having a pair of quadrature filters is that when their individual responses are squared and added together, we get a phase independent response. The magnitude response $OPmag$ and the phase response $OPphase$ are defined as:

$$OPmag = \sqrt{OPcos^2 + OPsin^2} \quad \text{Equation (7)}$$

$$OPphase = arctan(OPsin/OPcos) \quad \text{Equation (8)}$$

Consider a filterbank which contains 'M' filters and let $OP_{filter1}, OP_{filter2}, \ldots, OP_{filterM}$ be the magnitude response of the filter pairs of the filter bank, which are computed as shown in Equation 7. The overall output of the filter-bank is defined as the point-wise sum of the outputs of the individual filters of the filterbank. Let the overall output of the filter-bank be denoted by $OP_{overall}$ which is, given by the following equation:

$$OP_{overall} = OP_{filter1} + OP_{filter2} + \ldots\ldots + OP_{filter(M-1)} + OP_{filterM} \quad \text{Equation (9)}$$

To detect a SM or AD, the enhanced image would be filtered with a filter-bank and the overall output would be computed as described in Equation 9. If the filter-bank "matches" a SM or AD, a peak will be obtained at the spatial location corresponding to the center of the SM or AD. Thus, suspicious regions can be identified by detecting the local peaks in the overall output. Note that the larger the overall output at a particular spatial location, the higher the likelihood that the spatial location corresponds to the center of a SM or AD. We also note that we perform a point-wise addition and not a point-wise multiplication of the outputs of the individual filters. Point-wise multiplication is not used because even if one filter does not "match" a SM and has a low output then it would drastically affect the overall output of the filter-bank. Thus, by performing a point-wise addition, the output of a single filter will not drastically affect the overall output of the filter-bank. The procedure described above is repeated for all filter-banks and all the suspicious locations marked, across all filter-banks are collected and arranged in descending order according to the overall output values at those locations. From these, the first 'N' marks are selected as the possible locations of suspicious masses. To summarize, the aim in this detection step is to detect as many suspicious regions as possible and to achieve a high detection sensitivity. This may lead to a large number of FPI. This is acceptable as this is a stage one algorithm and the main focus is on the detection accuracy of the algorithm whereas the goal of stage two algorithms is to reduce the number of FPI.

2.3. Data Description

The images for this study were obtained from the Digital Database for Screening Mammography (DDSM) (http://marathon.csee.usf.edu/Mammography/Database.html) [25]. The DDSM is the largest publicly available data-set of digitized mammograms. To evaluate the performance of the algorithm, two sets of images were used for this study. One set contained 45 images with spiculated masses and the other set contained 45 images with architectural distortions. These images were scanned with a single digitizer and contained a single lesion and were randomly selected. All of the images were MLO view images. For the preliminary physical measurements, we randomly selected 6 cases of SM and 6 cases of AD from the DDSM. The selected cases had been digitized by a single scanner and represented a range of density ratings, subtlety ratings and pathology. Measurements were made separately from both the MLO and CC views. None of these cases were used in the evaluation of the detection algorithm and there was no overlap between the two groups of images.

2.4. Physical parameter measurements

We made measurements of several physical parameters of spiculated masses and architectural distortions. For this purpose, we have designed a simple prototype interface (Figure 7) and have conducted some preliminary measurements. Specifically, we use the ROI Manager plugin of NIH *ImageJ* (http://rsb.info.nih.gov/ij/) to enable a user, with minimal training, to place markers at specific locations, and compute the Euclidean (pixel) distance between the markers. This prototype allows for measurement of spicule width, at the base of the spicule (where it meets the mass, if any) as well as at other points along the spicule. The user can also measure the lesion dimensions of the central region along the principal axes. In addition, the operator can trace the spicule along its entire length in freeform, which delivers spicule length and enables the computation of such numerical measures as spicule tortuosity. Finally, the user can count the spicules associated with a lesion, and this measurement can be used to compute such essential statistics as angular density. Since the resolution of the images is known, the pixel measurements can be converted into physically meaningful quantities (*e.g.*, mm).

One of us (GJW) used NIH *ImageJ* to measure the length and the width at the base and the tip for six spicules randomly selected from each lesion. He also measured the length of the major and minor axes of the central region of each lesion. Finally, he counted the number of spicules that were visible for each lesion. In this study the measurements were made on a small set of images. In the future we will obtain measurements of the lesion parameters over a large number of cases, and this will provide the groundwork for our proposed evidence based paradigm for CAD/CADx.

2.5. Algorithm details

In this section, we describe how the physical measurements made are used to set the parameters of the detection algorithm. From our measurements of physical parameters of spiculated masses and architectural distortions, we observed that the average width of spicules is 17 pixels. For computational efficiency, we decimated the images by a factor of four and thus the average width of spicules is approximately 4 pixels. Thus, to detect peaks, each column of the Radon domain is convolved with the following filter: $[-1\ -1\ 1\ 1\ 1\ 1\ -1\ -1]^T$. Local peaks can be then be detected by thresholding the absolute value at each point in the filtered output. The threshold is defined as a percentage (p) of the maximum value in each column. We note that the coefficients at the center of the filter are positive and those at the periphery are negative and the sum of coefficients of the filter is zero. Thus, when this filter is over an area of constant or slowly varying gray levels, the output is zero or very small. We would like to emphasize that the choice of the filter used is based on the physical measurements observed.

To account for the variability in the shape and structure of SM and AD, filter-banks with different parameters are used. The parameters of the filter-banks were obtained from the physical measurements in the following manner. The mean, mean minus one standard deviation, and mean plus one standard deviation of the number of spicules per image was used to set possible values for parameter ω; the mean, mean minus one standard deviation, and mean plus one standard deviation of major and minor axis lengths (taken together) were used to set the possible values for parameter r_0. Thus, a total of 9 filterbanks were constructed. The ratio of the outer radius to the inner radius of each filterbank, and so parameter σ, was determined from the minimum value of the ratio of the average spiculation length to the average axis length.

In our preliminary studies, the algorithm marked the top 'N' strongest matches per image. A pixel was only marked as detected if it was more than a fixed distance from previously marked points; the distance was set by the maximum axes value measured in our preliminary study. By varying 'N', from 1 to 20, the tradeoffs in sensitivity and FPI can be visualized as an FROC curve.

3. RESULTS

	Spicule Length	Spicule Width (base)	Spicule Width (tip)	Major Axis	Minor Axis	Num. Spicule
SM	9.7±3.2	0.7±0.4	1.1±0.4	10.8±2.9	11.2±1.8	17±4
AD	17.3±9.7	1.1±0.7	1.1±0.7	17.6±6.8	15.5±5.0	20±6

Table 1. Average preliminary measurements (mm) made by the radiologist (GJW) (± standard deviation) across all spicules, all MLO images for SM and AD.

Table 1 shows the preliminary measurements made of several properties of SM and AD. The measurements made include the spicule length, spicule width at the base and tip of the spicule. The major and minor axes of the central mass regions and the number of spicules.

Figure 8 shows the results of the intermediate steps of the detection algorithm. Figures 8 (a) and (b) show the original image and a boundary containing a spiculated mass. This was marked by a radiologist and was obtained from the DDSM database. Figure 8 (c) shows the enhanced image obtained after applying the enhancement algorithm. This image is then filtered with RSFBs and the location of a potential lesion is taken to be the pixel that showed maximum response across all 9 filterbanks. The top six lesion candidates have been overlaid on the original image in Figure 8 (d). A true positive detection is defined as the marked pixel being within the ground truth outlined by the radiologist.

The algorithm was tested on 45 cases of SM and 45 cases of AD and the detection results of the algorithm are shown in Figure 9. This figure shows the FROC curves for the detection of spiculated masses and architectural distortions. We achieved a sensitivity of 80% at 14 FPI for architectural distortions and 91% at 12 FPI for spiculated masses. These results are competitive with existing stage-one algorithms.

4. DISCUSSION and CONCLUSION

In this paper we present preliminary results in support of our development of an evidence based framework for the detection of SM and AD based on their physical characteristics. A new stage one method for the detection of spiculated masses and architectural distortions was presented. The two steps of the algorithm which included an enhancement step and a detection step were discussed in detail. The key idea in the enhancement step is the application of a filter in the Radon domain. For the detection step, a new class of linear image filters developed by us specifically for SMs and ADs called Radial Spiculation filters were introduced. These filters are highly specific narrowband filters and form a new class of wavelet-type filterbanks derived from optimal theories of filtering The unique and pioneering method of basing the filter parameters on actual measurements of physical characteristics of SMs and ADs enabled us to produce results that are competitive with existing stage-one methods. We would like to emphasize that we have presented a stage one algorithm only and the main focus was the detection of the maximum number of potential lesions. We acknowledge that currently, the number of FPI is high and we are actively developing a stage-two algorithm to reduce the number of FPI. We believe that the physical measurements would also help us develop new strategies and features for the task of false positive reduction.

One limitation of our algorithm is that the enhancement step enhances all linear structures which would have a width similar to that of spicules. As the Radon transform is a "global transform" it can detect the presence or absence of lines but cannot determine the spatial locations of line segments. One way to overcome this would be too use some for of a local Radon transform. Another limitation of the current study is that the measurements were made on a small number of cases and thus we are planning to make many more measurements which will serve as a solid foundation for our evidence based approach to detection of abnormalities. A comprehensive set of statistics of the physical parameters of SM and AD could be used be used not only for improving detection algorithms but also for more localized tasks such as diagnosis and reduction of false positives. We strongly believe that the systematic study and quantification of the physical parameters of SM and AD would not only be useful for our developmental efforts but also for those of future researchers in computer-aided detection and diagnosis.

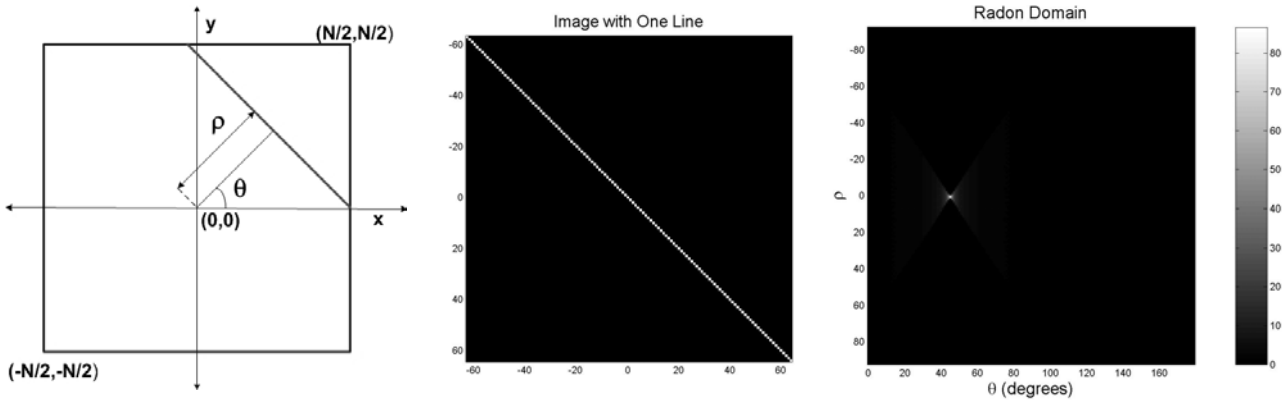

Figure 1. Parameters of the Radon transform *(ρ,θ)* (Left), An image with a single line (Center) and the corresponding Radon Domain of the image (Right)

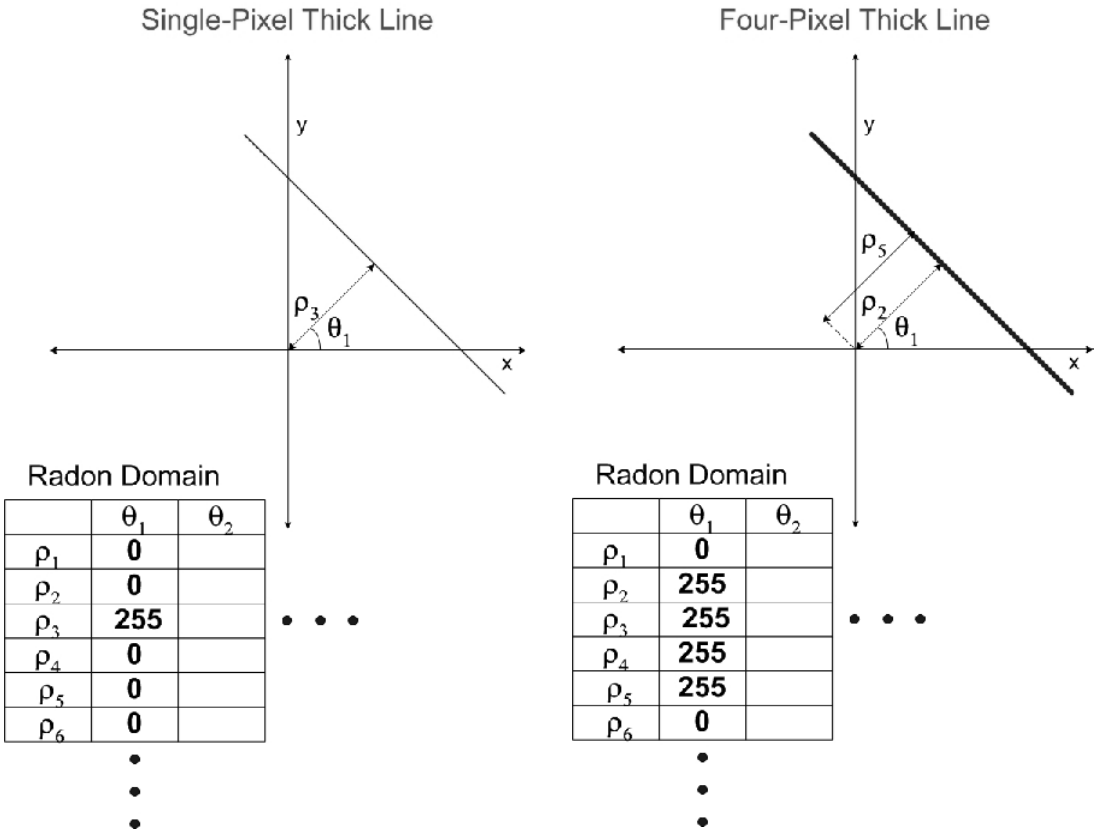

Figure 2. (a) A single pixel thick line (Left) (b) A four pixel thick line (Right) and sections of their Radon transforms. A line in an image maps to a peak of a particular width in the Radon domain.

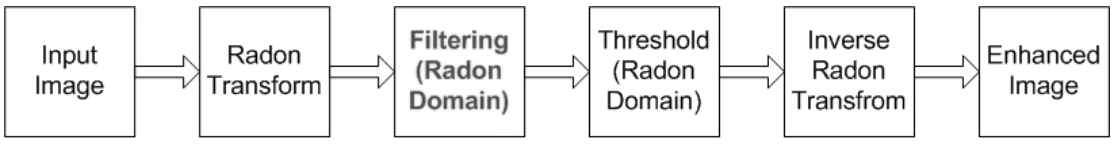

Figure 3. A block diagram of the steps involved in the enhancement of spicules. The key idea is that we can enhance "local peaks" by filtering the columns in the Radon domain. In Figure 4 we demonstrate the benefits of filtering in the Radon domain.

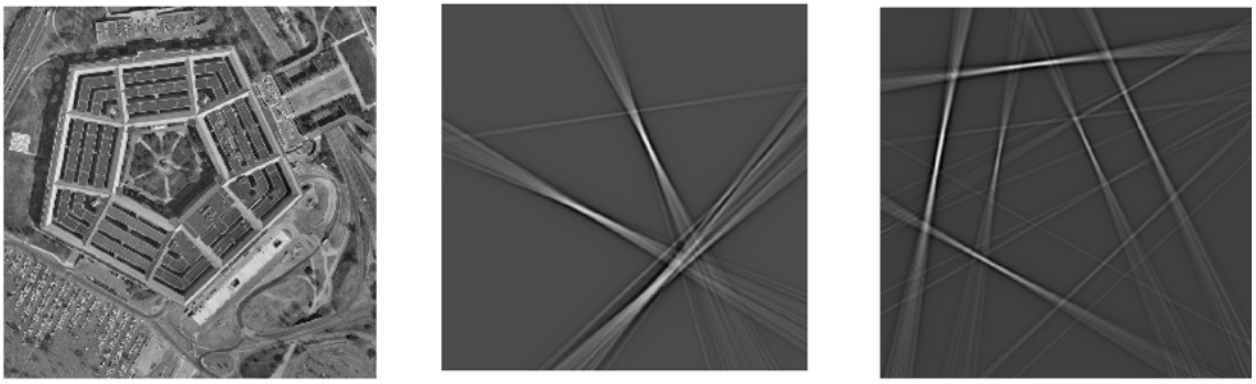

(a) Original Image

(b) Enhanced Image (without Filtering in the Radon Domain)

(c) Enhanced Image (with Filtering in the Radon Domain)

Figure 4. Advantages of Filtering in the Radon Domain: Results obtained at the end of the enhancement algorithm. In figures (a) and (b) thresholding was carried out so that the same of coefficients were present after thresholding.

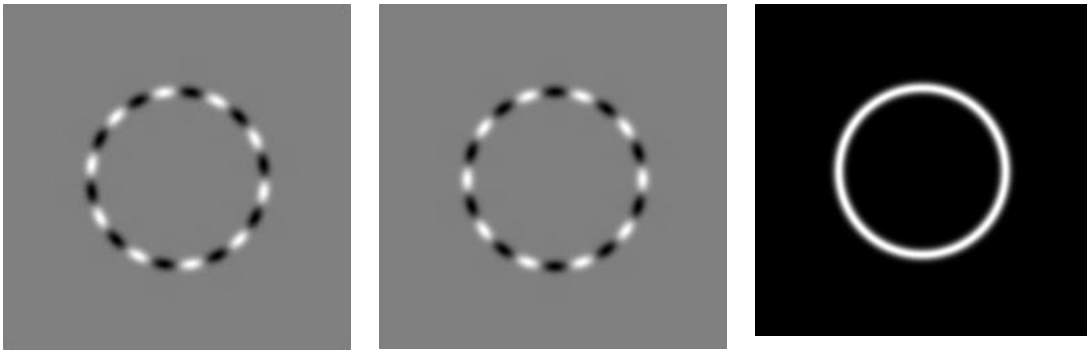

Figure 5. Example of a Radial Spiculation Filter (RSF). (Left) Cosine part of the RSF; (Middle) Sine part of the RSF; (Right) Gaussian envelope of the RSF.

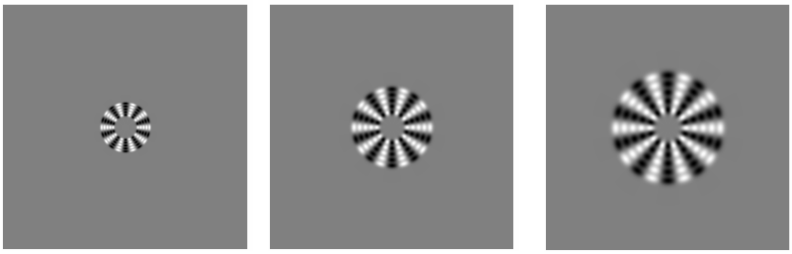

Figure 6. Three Radial Spiculation Filterbanks, each composed of five RSFs of progressively increasing radii but matching radial frequencies. Each of the above RSFBs has the same inner radius but different outer radius. These would correspond to lesions where the central mass is the same size but the spicule lengths differ.

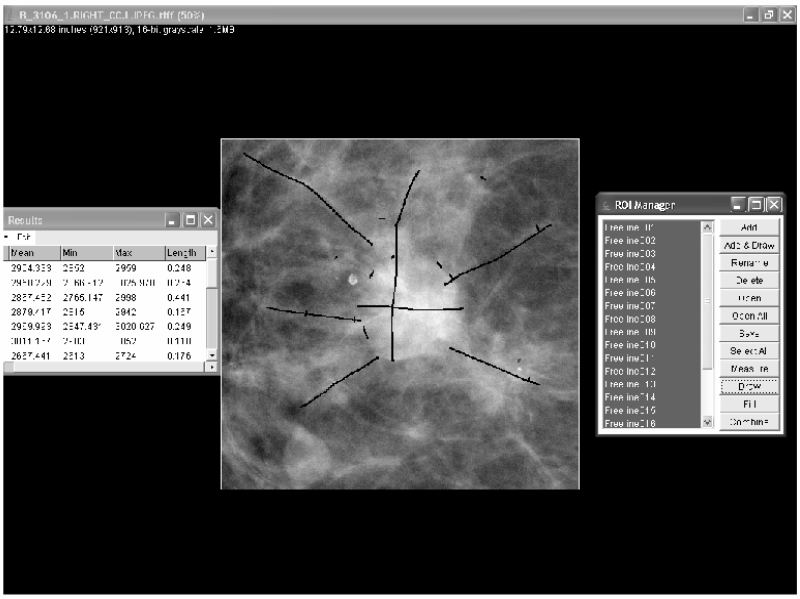

Figure 7. Prototype interface for obtaining measurements of key characteristics of spiculated lesions. Measurements were collected with the lights dimmed.

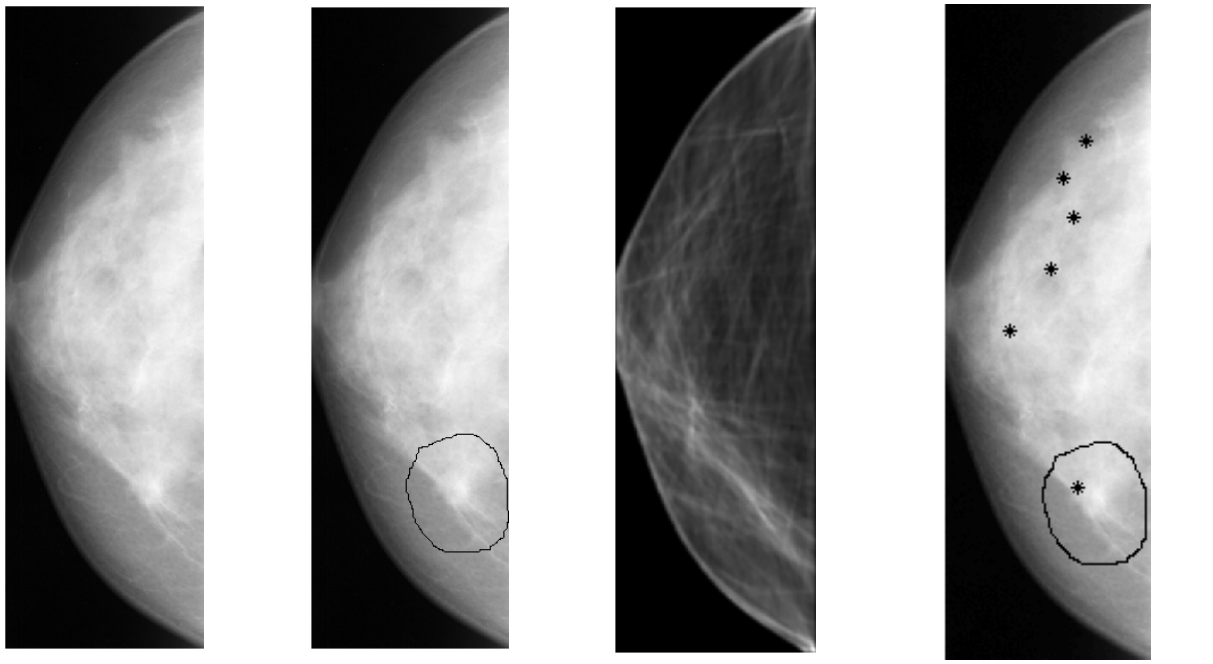

(a) Original image.

(b) Ground truth: original image with a boundary containing the spiculated lesion overlaid.

(c) Enhanced Image. Output obtained from the enhancement step of the algorithm.

(d) Detection results obtained (the 6 largest marks are overlaid on the original image).

Figure 8. Steps of the detection algorithm. Figures (a) and (b) show the original image and the ground truth overlaid on it. Figure (c) shows the enhanced image and finally Figure (d) shows the outputs of the detection algorithm with the 6 largest marks overlaid.(Image C_0015_1.RIGHT_CC from Volume: cancer_01,Case:C-0015-1 in DDSM).

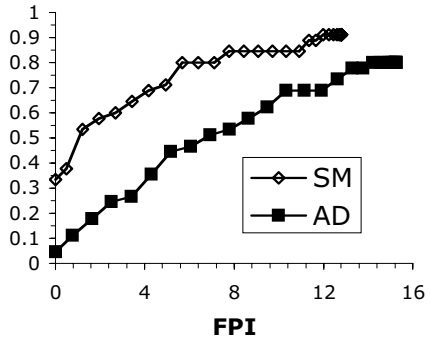

Figure 9. FROC curves based on 45 images of SM and 45 images of AD for the initial version of our stage 1 detection algorithm using preliminary estimates for parameter values.

REFERENCES

[1] "Cancer Facts and Figures 2004," American Cancer Society, Atlanta 2004.

[2] E. J. Feuer, L. Wun, C. C. Boring, W. D. Flanders, M. J. Timmel, and T. Tong, "The Lifetime Risk of Developing Breast Cancer," *Journal of the National Cancer Institute*, vol. 85, pp. 892-897, 1993.

[3] L. Wun, R. M. Merrill, and E. J. Feuer, "Estimating Lifetime and Age-Conditional Probabilities of Developing Cancer," *Lifetime Data Analysis*, vol. 4, pp. 169-186, 1998.

[4] American College of Radiology, *ACR BI-RADS - Mammography, Ultrasound & Magnetic Resonance Imaging*, Fourth ed. Reston, VA: American College of Radiology, 2003.

[5] S. G. Orel, N. Kay, C. Reynolds, and D. C. Sullivan, "BI-RADS categorization as a predictor of malignancy," *Radiology.*, vol. 211, pp. 845-50, 1999.

[6] C. H. Lee, "Screening mammography: proven benefit, continued controversy," *Radiologic clinics of North America*, vol. 40, pp. 395-407, 2002.

[7] K. Kerlikowske, P. A. Carney, B. Geller, M. T. Mandelson, S. H. Taplin, K. Malvin, V. Ernster, N. Urban, G. Cutter, R. Rosenberg, and R. Ballard-Barbash, "Performance of screening mammography among women with and without a first-degree relative with breast cancer," *Annals of Internal Medicine*, vol. 133, pp. 855-63, 2000.

[8] T. M. Kolb, J. Lichy, and J. H. Newhouse, "Comparison of the performance of screening mammography, physical examination, and breast US and evaluation of factors that influence them: an analysis of 27,825 patient evaluations.[see comment]," *Radiology*, vol. 225, pp. 165-75, 2002.

[9] R. E. Bird, T. W. Wallace, and B. C. Yankaskas, "Analysis of cancers missed at screening mammography," *Radiology.*, vol. 184, pp. 613-7, 1992.

[10] M. L. Giger, "Computer-aided diagnosis in radiology.[comment]," *Academic Radiology*, vol. 9, pp. 1-3, 2002.

[11] D. B. Kopans, "The positive predictive value of mammography," *AJR. American Journal of Roentgenology*, vol. 158, pp. 521-6, 1992.
[12] M. L. Giger, "Computer-aided diagnosis of breast lesions in medical images," *Computing in Science & Engineering*, vol. 2, pp. 39-45, 2000.
[13] M. L. Giger, N. Karssemeijer, and S. G. Armato, III, "Computer-aided diagnosis in medical imaging," *IEEE Transactions on Medical Imaging*, vol. 20, pp. 1205-1208, 2001.
[14] K. Doi, H. MacMahon, S. Katsuragawa, R. M. Nishikawa, and Y. Jiang, "Computer-aided diagnosis in radiology: potential and pitfalls," *European Journal of Radiology.*, vol. 31, pp. 97-109, 1999.
[15] C. J. Vyborny, M. L. Giger, and R. M. Nishikawa, "Computer-aided detection and diagnosis of breast cancer," *Radiologic Clinics of North America*, vol. 38, pp. 725-40, 2000.
[16] M. P. Sampat, M. K. Markey, and A. C. Bovik, "Computer-Aided Detection and Diagnosis in Mammography," in *Handbook of Image and Video Processing*, A. C. Bovik, Ed., 2nd ed, 2005.
[17] L. Liberman, A. F. Abramson, F. B. Squires, J. R. Glassman, E. A. Morris, and D. D. Dershaw, "The breast imaging reporting and data system: positive predictive value of mammographic features and final assessment categories," *AJR. American Journal of Roentgenology.*, vol. 171, pp. 35-40, 1998.
[18] U. S. F. a. D. Administration, "Summary of Safety and Effectiveness Data: R2 Technologies," *P970058*, 1998.
[19] C. J. Vyborny, T. Doi, K. F. O'Shaughnessy, H. M. Romsdahl, A. C. Schneider, and A. A. Stein, "Breast cancer: importance of spiculation in computer-aided detection," *Radiology.*, vol. 215, pp. 703-7, 2000.
[20] H. Burrell, D. Sibbering, and A. Wilson, "Screening interval breast cancers: Mammograhic features of prognostic factors.," *Radiology*, vol. 199, pp. 811-817, 1996.
[21] H. Burrell, A. Evans, A. Wilson, and S. Pinder, "False-negative breast screening assessment. What lessons can we learn?," *Clinical Radiology*, vol. 56, pp. 385-388, 2001.
[22] J. A. Baker, E. L. Rosen, J. Y. Lo, E. I. Gimenez, R. Walsh, and M. S. Soo, "Computer-aided detection (CAD) in screening mammography: sensitivity of commercial CAD systems for detecting architectural distortion," *AJR. American Journal of Roentgenology.*, vol. 181, pp. 1083-8, 2003.
[23] A. Rosenfeld and A. C. Kak, *Digital Picture Processing*, vol. 1: Academic Press, 1982.
[24] D. B. Kopans, *Breast Imaging*: Lippincott-Raven Publishers, Philadelphia, 1998.
[25] M. Heath, K. W. Bowyer, and D. Kopans, "Current status of the Digital Database for Screening Mammography," presented at Digital Mammography, Dordrecht, 1998.